Comparative Study of Cogging Torque, Torque Ripple, and Vibration on Stator Tooth Chamfer Types in Permanent Magnet Synchronous Motors

Yun-Jae Won[1], Jae-Hyun Kim[2,3], Soo-Min An[1], and Myung-Seop Lim[2]

[1]Department of Automotive Engineering (Automotive-Computer Convergence), Hanyang University, Seoul 04763, Republic of Korea
[2]Department of Automotive Engineering, Hanyang University, Seoul 04763, Republic of Korea
[3]School of Mechanical Engineering, Yeungnam University, Daegu 38541, Republic of Korea

The high power density, high efficiency, and wide speed range of permanent magnet synchronous motors (PMSMs) are attractive features. However, the cogging torque and unsuppressed torque ripple of PMSMs degrade torque quality and reliability and cause vibration. This article compares the effectiveness of PMSMs in reducing the cogging torque, torque ripple, and vibration by applying each stator tooth chamfer types: inner eccentricity chamfer, outer eccentricity chamfer, linear chamfer, and circular chamfer. First, stator tooth chamfers were applied to the reference model to confirm the tendency of cogging torque, torque ripple, and electromagnetic force according to the design variables by chamfer types, and it was demonstrated that the chamfer needs to be applied in a way that reduces the harmonics of the air-gap magnetic flux density to improve the performances through finite element analysis (FEA). Next, the optimum design for reducing cogging torque, torque ripple, and electromagnetic force was performed for each stator tooth chamfer types for a valid comparison. As a result, it was confirmed that there are advantageous stator tooth chamfer types based on each performance. Finally, a prototype was fabricated and tested to validate the FEA results of the optimum model for performance comparison.

***Index Terms*— Cogging torque, electromagnetic force, permanent magnet synchronous motors (PMSMs), stator tooth chamfer, torque ripple, vibration.**

I. Introduction

PERMANENT magnet synchronous motors (PMSMs) are widely used in the automotive industry due to their high power density, high efficiency, and wide speed range, compared to the traditionally used induction motors (IMs) in industrial motors [1]. However, PMSMs suffer from cogging torque owing to the permanent magnets (PMs) with a constant magnetomotive force regardless of the load condition, resulting in a relatively large torque ripple and consequent mechanical vibration. It is essential to reduce cogging torque, torque ripple, and vibration for PMSMs used in applications that require precise control and smooth motion. Indeed, many studies have been conducted on reduction method and principle of cogging torque, torque ripple, and vibration. It is demonstrated that cogging torque reduction can be achieved by varying the design variables related to PMs [2]. Also, a novel composed T-shaped notching rotor was studied to reduce cogging torque and harmonics components that cause torque ripple [3]. However, since a design tradeoff is found between cogging torque and torque ripple, and local saturation of the tooth tip causes an increase in cogging torque and torque ripple, a suitable slot opening width and tooth tip thickness should be selected [4]. In [5], the correlation between electromagnetic force and vibration is analyzed and methods for vibration and noise reduction are presented. According to previous studies, there is a tradeoff between cogging torque, torque ripple, and vibration depending on design variables, so it is necessary to design according to the application of PMSMs. The performance requirements of PMSMs vary depending on the different applications.

Therefore, this article classifies four types of chamfers that can be applied to the conventional stator tooth structure and proposes which type of stator tooth chamfer should be applied to optimize each performance through a comparative study. First, the geometry and parameters of each stator chamfer types were illustrated, and then, the tendency of cogging torque, torque ripple, and electromagnetic force were shown when each chamfer was applied to the reference model. Subsequently, the optimum design was performed for each stator chamfer type to compare which type of chamfer is effective for each performance. Finally, the chamfer type that is effective in improving each performance was presented and a prototype was fabricated to verify the results.

II. Stator Tooth Chamfer Types and Chamfer Application Effects

A. Stator Tooth Chamfer Types

Fig. 1 shows the chamfer types and corresponding parameters applied to the stator tooth. The inner and outer eccentricity chamfers, types 1 and 2, are applied with a radial eccentricity from the inside and outside of the stator tooth to the tooth center, where $r_{i,\mathrm{ecc}}$ and $r_{o,\mathrm{ecc}}$ are the length of the inner and outer eccentricity in the radial direction. Especially, type 1 is

Manuscript received 24 March 2024; revised 25 May 2024; accepted 8 June 2024. Date of publication 11 June 2024; date of current version 27 August 2024. Corresponding author: M. -S. Lim (e-mail: myungseop@hanyang.ac.kr).

Color versions of one or more figures in this article are available at https://doi.org/10.1109/TMAG.2024.3412965.

Digital Object Identifier 10.1109/TMAG.2024.3412965

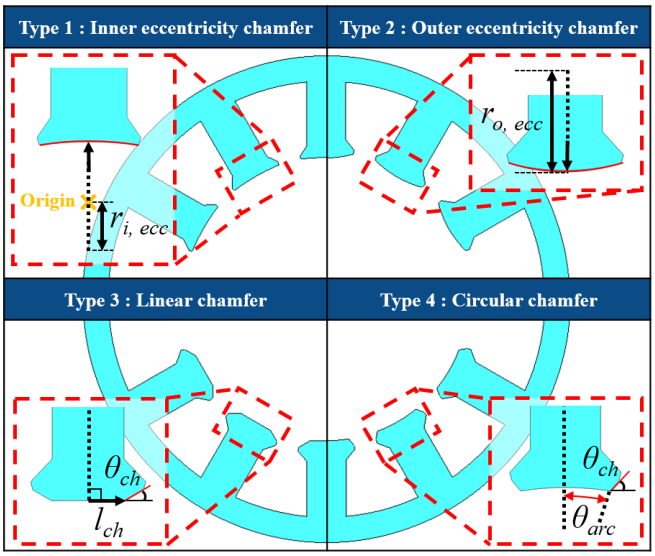

Fig. 1. Stator tooth chamfer types and corresponding parameters.

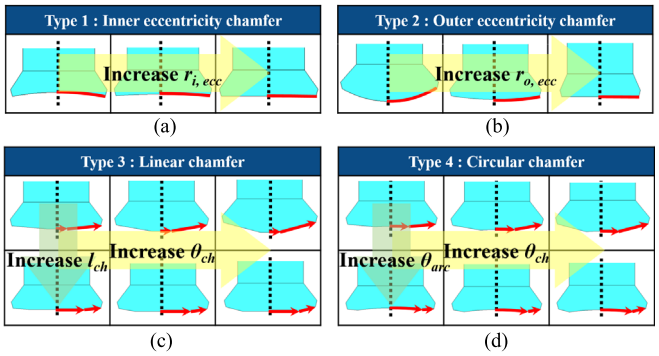

Fig. 2. Tooth tip geometry based on changing variables by stator tooth chamfer types. (a) Inner eccentricity chamfer. (b) Outer eccentricity chamfer. (c) Linear chamfer. (d) Circular chamfer.

applied with $r_{i,\mathrm{ecc}}$ opposite to the origin of the corresponding tooth tip. The linear chamfer, type 3, is chamfered by chamfer length and angle along a straight line tangentially from the center of the tooth tip, where l_{ch} is the chamfer length indicating the chamfer position and θ_{ch} is the chamfer angle. The circular chamfer, type 4, is chamfered by chamfer arc and angle in a circumferential direction from the tooth tip center, where θ_{arc} is the chamfer arc indicating the chamfer position.

The four types of stator tooth chamfers include different chamfer shapes, as shown in Fig. 2, based on the range of variables that can be applied to stator tooth structure for manufacturability considerations. Types 1 and 2 can cover both concave and convex chamfers at the stator tooth tip. In addition, type 3 has a flat tooth tip and a chamfered end at a specific angle, and type 4 has a conventional tooth tip with a chamfered end at a specific angle.

B. Chamfer Application Effects

In this part, the effect of stator chamfer application was verified using finite element analysis (FEA), and the tendency of cogging torque, torque ripple, and electromagnetic force according to chamfer variables was analyzed. The analysis is performed by applying the stator tooth chamfer types to a reference model, which has a conventional tooth tip with no chamfer. The specifications of the reference model are presented in Table I. Fig. 3 shows a comparison of the air-gap

TABLE I
REFERENCE MODEL SPECIFICATIONS

Parameters	Values	Unit
Number of poles / slots	8 / 12	-
DC link voltage	12.0	V_{dc}
Current limit	40.0	A_{rms}
Current density	15.0	A_{rms}/mm^2
Slot fill factor	45.0	%
PM remanence	1.39	T(@20°C)
Stator diameter	86.0	mm
Air gap length	1.0	mm
Stack length	18.0	mm
Two step-skew angle	7.5	°
Rated speed	1000	rpm
Rated torque	2.1	Nm

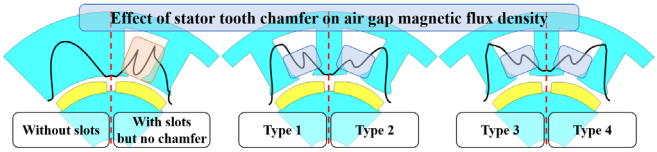

Fig. 3. Air-gap magnetic flux density waveform applying stator tooth chamfer by types to reference model.

magnetic flux density waveforms without slots, with slots but no chamfers, and with each type of stator tooth chamfer applied to the reference model. The stator chamfer increases the effective air-gap length and reduces the rate of change of the air-gap permeance with spatial position, which reduces the harmonic magnitude of the air-gap magnetic flux density. Since the reduction in harmonics of the air-gap flux density leads to an improved in the performance of cogging torque, torque ripple, and vibration, chamfers should be applied in the way that its harmonics are reduced. Cogging torque is the reluctance torque that opposes rotation when the rotor is aligned with the stator tooth. Torque ripple is also cused by the changes in magnetic field strength as the rotor rotates. In addition, vibration is caused not only by cogging torque and torque ripple but also by electromagnetic forces resulting from the interaction between the magnetic fields generated by the stator windings and the PMs of the rotor. Especially, the radial vibration can be enhanced or weakened by tangential as well as radial electromagnetic force [6]. In addition, electromagnetic force harmonics with low mode numbers can cause high mechanical vibrations in PMSMs with fractional slot combinations [7]. To improve vibration performance, radial and tangential electromagnetic forces and electromagnetic force total harmonic distortion (THD) should also be considered.

Therefore, chamfers that reconfigure the magnetic field distribution to improve magnetic flux density uniformity seem to be effective in reducing cogging torque, torque ripple, and electromagnetic force when applied optimally. The performance tendency of peak-to-peak cogging torque, torque ripple, and second electromagnetic force, electromagnetic force THD in radial and tangential directions, calculated using FEA according to chamfer variables, is shown in Fig. 4 when the reference model is applied with different types of stator tooth chamfer. Based on the reference model, it can be seen that all performances except tangential electromagnetic force improve as the inner eccentricity increases when type 1 is applied. When type 2 is applied, only tangential electromagnetic force

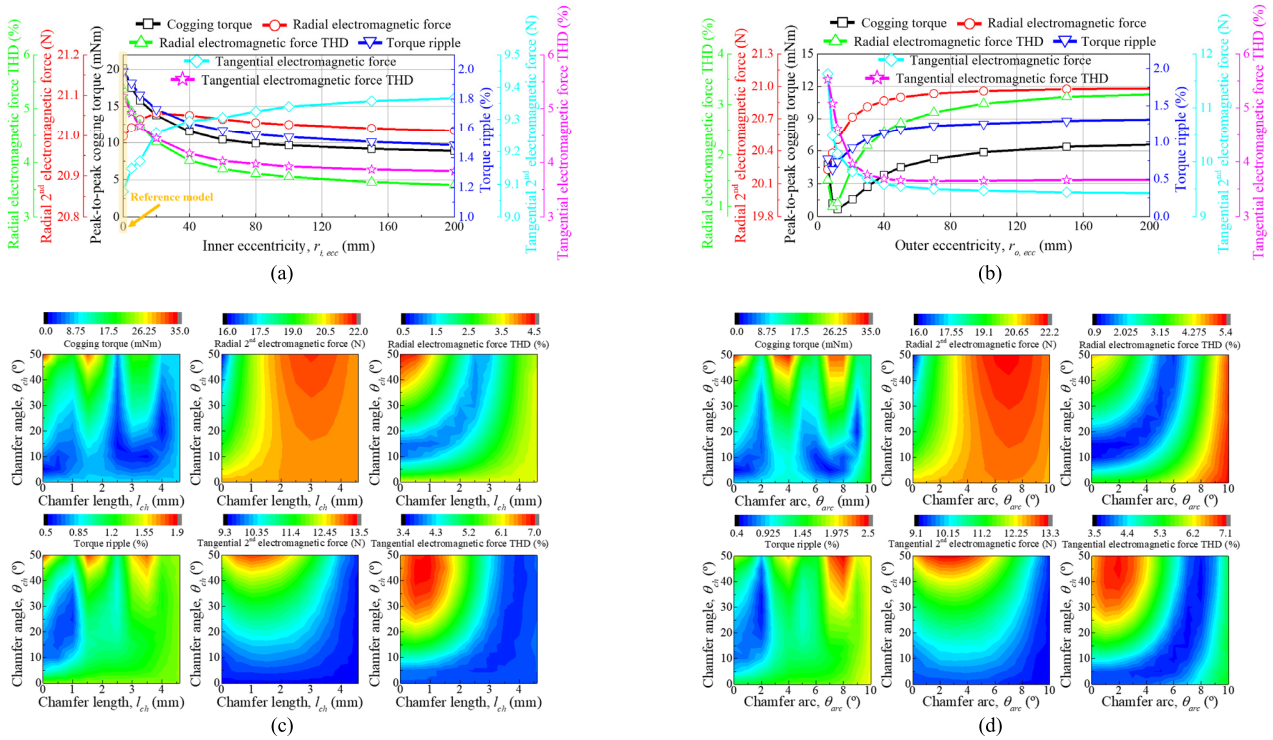

Fig. 4. Performance tendency depending on chamfer variables by chamfer types based on the reference model. (a) Inner eccentricity chamfer. (b) Outer eccentricity chamfer. (c) Linear chamfer. (d) Circular chamfer.

and THD improve as the outer eccentricity increases. When types 3 and 4 are applied, the performances have similar tendency depending on the chamfer variables. Therefore, it is confirmed that the behavior of cogging torque, torque ripple, electromagnetic force, and THD is significantly changed depending on the variables of stator tooth chamfer types, and optimum design for each stator tooth chamfer type is required to improve each performance. In other words, the parameters for each chamfer types should be included in the design variables for optimum design to reduce cogging torque, torque ripple, and vibration. The cogging torque in PMSMs can be expressed as [3]

$$T_{\mathrm{cog}}(\alpha) = -\frac{\pi z L_a}{4\mu_0}\left(R_{\mathrm{is}}^2 - R_{\mathrm{or}}^2\right)\sum_{l=1}^{\infty} m G_l B_{rn} \sin(lz\alpha) \tag{1}$$

where T_{cog} is the cogging torque, α is the relative position of pole and tooth, μ_0 is the permeability of vacuum, z is the slot number, L_a is the axial length of the PMSMs, R_{is} is the inner radius of the stator, R_{or} is the outer radius of the rotor, G_l is the lth Fourier transform coefficients of the PM geometry parameter, and B_{rn} is the nth Fourier transform coefficients of the distribution of air-gap flux density. The cogging torque was calculated as the peak-to-peak of the maximum subtracted from the minimum of the cogging torque waveform. For the assumption of a three-phase sinusoidal current, the torque harmonics, in terms of magnetic torque only, can be expressed as follows:

$$T_m = \frac{3}{2\omega_m}\left[E_1 I_1 + \sum_{n=6k}(-E_{n-1} + E_{n+1}) I_1 \cos np\omega_m t\right] \tag{2}$$

where T_m is the magnetic torque, ω_m is the mechanical angular velocity, E_n is the nth amplitude of the induced voltage

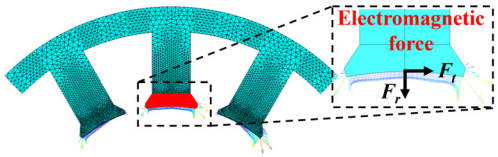

Fig. 5. Electromagnetic force calculation area.

harmonic, I_1 is the amplitude of the fundamental wave current, k is the natural number, p is the pole-pair, and t is the time. Torque ripple in the torque waveform under the rated load condition was calculated by dividing the peak-to-peak of the waveform by the average torque. The local electromagnetic force F_s^i applying on a given node i can be written as [8]

$$F_s^i = \sum_{\forall e |\, i \in e}\int_e \left(-\mathbf{B}^T \cdot \mathbf{J}^{-1} \cdot \frac{\partial \mathbf{J}}{\partial s} \cdot \mathbf{H} + \frac{\mu}{2}|\mathbf{H}|^2 |\mathbf{J}^{-1}| \frac{\partial |\mathbf{J}|}{\partial s}\right) dV \tag{3}$$

where e is the mesh element, $\mathbf{B}$ is the magnetic flux density vector, $\mathbf{H}$ is the magnetic field vector, $\mathbf{J}$ is the Jacobian matrix of the element e, s is the direction domain, μ is the permeability of material, and V is the volume. The electromagnetic force waveform was extracted by summing the electromagnetic force in the stator tooth tip region by element and equalizing it in the radial and tangential directions to obtain an electromagnetic force waveform, as shown in Fig. 5. Then, the fundamental wave of the electromagnetic force waveform, which is the second-order component, was calculated by fast Fourier transform (FFT), and the THD was calculated. Based on the formulas for each performance, the design variables for the optimum design process in Section III were selected.

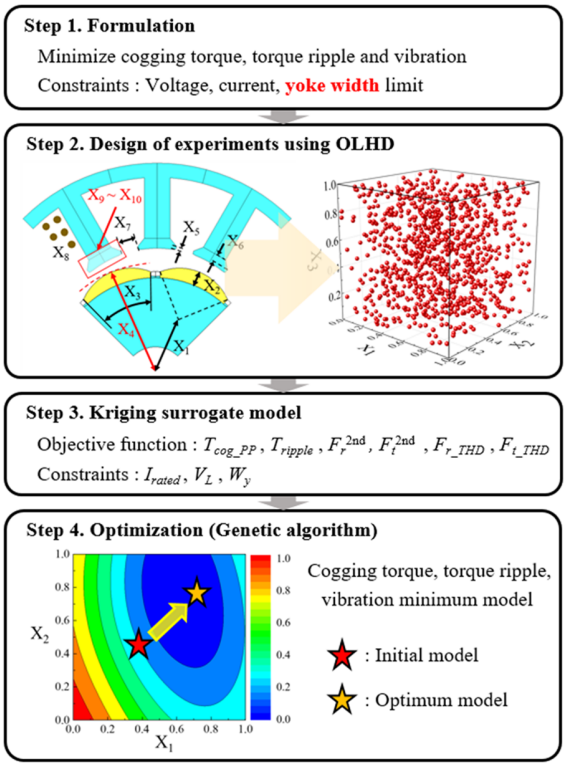

Fig. 6. Optimum design process.

III. Optimum Design for Performance Comparison by Stator Tooth Chamfer Types

In this section, the optimum design was performed to minimize cogging torque, torque ripple, and vibration for different types of stator chamfers, and the performances of the four designed optimum models were compared. Four optimum designs are performed for each stator tooth chamfer type, and the chamfer variable is added to each optimum design. The design specifications are the same as Table I of the reference model presented previously.

A. Design Process and Optimization

Fig. 6 illustrates the overall optimum design process to minimize cogging torque, torque ripple, radial and tangential electromagnetic forces, and THD for vibration reduction while satisfying the constraints. First, in the formulation step, the objective function and constraints are defined to compare the cogging torque, torque ripple, and vibration of the optimally designed PMSMs based on the stator tooth chamfer types. Especially, the yoke width, considered to have a significant impact on vibration, was designed to be equal for fair comparison. The optimization problem is expressed as follows:

$$\begin{aligned} \min\ & T_{\text{cog\_PP}},\ T_{\text{ripple}},\ F_r^{2\text{nd}},\ F_t^{2\text{nd}},\ F_{r\_\text{THD}},\ F_{t\_\text{THD}} \\ \text{s.t.}\ & I_{\text{rated}} \le I_{\text{limit}} \\ & V_L \le V_{L\_\max} \\ & W_y = W_{y\_\text{limit}} \end{aligned} \tag{4}$$

where $T_{\text{cog\_PP}}$ is the peak-to-peak of the cogging torque, T_{ripple} is the torque ripple, $F_r^{2\text{nd}}$ and $F_t^{2\text{nd}}$ are the radial and tangential second electromagnetic force, respectively, F_{r_THD} and F_{t_THD} are the radial and tangential electromagnetic force THD, respectively, I_{rated} is the rated current to generate the rated torque, I_{limit} is the current limit, V_L is the line-to-line voltage, $V_{L\_\max}$ is the maximum line-to-line voltage, W_y is the yoke width, and W_{y_limit} is the yoke width limit. Second, design variables sensitive to each performance were selected, as shown in Fig. 7, and experimental points were extracted using an optimal Latin hypercube design (OLHD), which distributes the experimental points, so that the minimum distance between the points is maximized over the range of the design variables. Third, a kriging surrogate model was constructed to predict the peak-to-peak cogging torque, torque ripple, radial and tangential second electromagnetic force, and radial and tangential electromagnetic force THD selected as objective functions and the rated current, line-to-line voltage, and yoke width selected as constraints. Finally, the genetic algorithm was used to minimize the cogging torque, torque ripple, second electromagnetic force, and electromagnetic force THD with equal weights while satisfying the constraints, resulting in the optimum model for each stator tooth chamfer type.

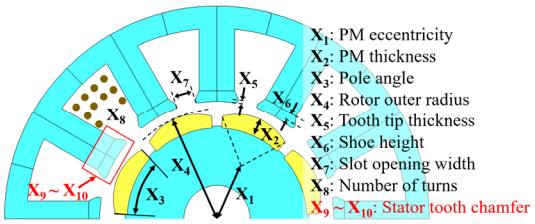

Fig. 7. Design variables.

TABLE II
FEA Results of the Optimum Design Models by Chamfer Types

Performances	Type 1	Type 2	Type 3	Type 4
Peak-to-peak cogging torque (mNm)	6.7	11.0	13.1	3.1
Torque ripple (%)	3.17	3.75	1.6	2.1
Radial electromangtic force (N)	22.59	19.79	21.53	21.35
Tangential electromagnetic force (N)	11.27	10.83	12.4	11.9
Radial electromagnetic force THD (%)	5.71	1.6	3.01	1.39
Tangential electromagnetic force THD (%)	3.1	2.98	1.7	2.97
Maximum radial displacement (μm)	0.170	0.148	0.166	0.151

B. Design Results

Table II shows the results of the optimally designed models for each stator tooth chamfer types. In terms of cogging torque, it is most effective in the order of type 4, type 1, type 2, and type 3. In addition, in terms of torque ripple, it is most effective in the order of type 3, type 4, type 1, and type 2. Finally, in terms of radial displacement, which is a vibration performance, it is most effective in the order of type 2, type 4, type 3, and type 1. The type 4 model, which is relatively the most effective for cogging torque, torque ripple, and vibration performance, was fabricated for experimental verification.

IV. Experimental Verification

A prototype was fabricated, as shown in Fig. 8(a), and tested using a cogging torque meter and a load motor, as shown in Figs. 8(b) and 9. By measuring the cogging torque of the fabricated prototype, it was confirmed that the harmonic order

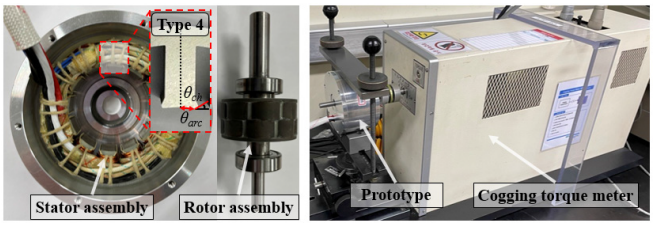

(a) (b)

Fig. 8. Optimum model prototype for type 4 consisting of (a) stator and rotor assembly and (b) cogging torque test setup.

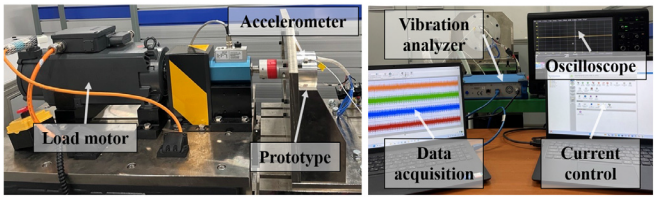

Fig. 9. Load and vibration test setup.

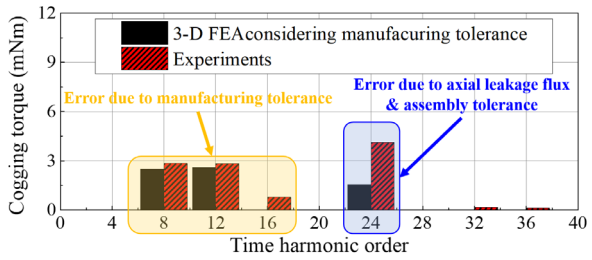

Fig. 10. FEA and test results of cogging torque.

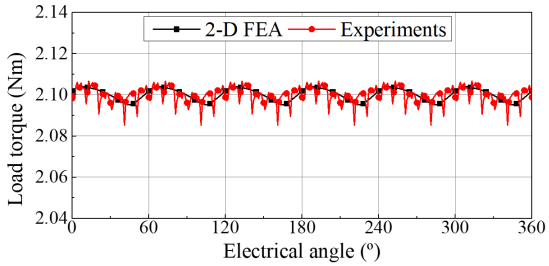

Fig. 11. FEA and test results of torque ripple under rated load condition.

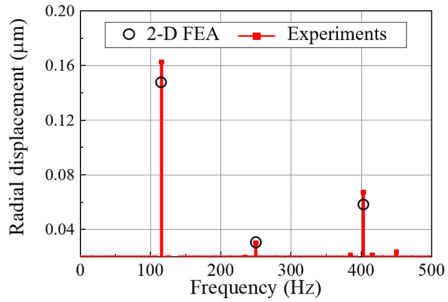

Fig. 12. FEA and test results of vibration under rated load condition.

of the number of poles and slots due to the manufacturing tolerance occurred, and when the tolerance was modeled in FEA, the cogging torque result was similar, as shown in Fig. 10. The error in the 24th cogging torque with step-skew between 3-D FEA and experiments of the type four model is caused by the axial leakage flux and the assembly tolerance of the skew angle [9]. In addition, the torque ripple under rated load condition was measured, and it was confirmed that the torque waveforms of FEA and experiments were similar, as shown in Fig. 11. Finally, the vibration was measured, and it was confirmed that the vibrations of FEA and experiments were similar, with the largest vibration amplitude at second-order rotational frequency, as shown in Fig. 12. To analyze the low-frequency vibration, the time-domain acceleration was converted to the frequency domain and the average acceleration was calculated. To calculate the radial displacement, the acceleration was divided by the square of each respective frequency.

V. Conclusion

This article compares which type of stator tooth chamfer is effective in reducing cogging torque, torque ripple, and vibration. First, four types of stator tooth chamfers were selected by considering the diversity of stator tooth tip geometries. Accordingly, the effects of each stator tooth chamfer on the cogging torque, torque ripple, and vibration when applied to the reference model were verified by FEA. It was confirmed that the cogging torque, torque ripple, and vibration could be reduced by applying the chamfer types, and the optimal design was proceeded. In optimum design, cogging torque and torque ripple, as well as the second electromagnetic force and electromagnetic force THD in the radial and tangential directions affecting vibration were set as the objective functions, and four optimum models for each chamfer types were derived that minimized each performance while satisfying the constraints. By comparing the performances of these optimized models, it was confirmed that chamfer type 4 is favorable for reducing cogging torque, type 3 for reducing torque ripple, and type 2 for reducing vibration.

Acknowledgment

This work was supported in part by the Korea Institute of Energy Technology Evaluation and Planning (KETEP) grant funded by the Korea Government (MOTIE) under Grant RS-2023-00232593 and in part by the Development of Common Base Technology for Medium Power Industrial Motors.

References

[1] A. Krings and C. Monissen, "Review and trends in electric traction motors for battery electric and hybrid vehicles," in *Proc. Int. Conf. Electr. Mach. (ICEM)*, Gothenburg, Sweden, Aug. 2020, pp. 1807–1813.

[2] T. Li and G. Slemon, "Reduction of cogging torque in permanent magnet motors," *IEEE Trans. Magn.*, vol. 24, no. 6, pp. 2901–2903, Nov. 1988.

[3] B. Wang, D. Wang, C. Peng, C. Wang, C. Xu, and X. Wang, "Interior permanent magnet synchronous machines with composed T-shaped notching rotor," *IEEE Trans. Ind. Electron.*, vol. 71, no. 6, pp. 5519–5529, Jun. 2024.

[4] D. Wu and Z. Q. Zhu, "Design tradeoff between cogging torque and torque ripple in fractional slot surface-mounted permanent magnet machines," *IEEE Trans. Magn.*, vol. 51, no. 11, pp. 1–4, Nov. 2015.

[5] S. Zuo, F. Lin, and X. Wu, "Noise analysis, calculation, and reduction of external rotor permanent-magnet synchronous motor," *IEEE Trans. Ind. Electron.*, vol. 62, no. 10, pp. 6204–6212, Oct. 2015.

[6] M. Liu, J. Zou, Y. Xu, H. Lan, and G. Yu, "Vibration enhancement or weakening effect caused by permanent magnet synchronous motor radial and tangential force formed by tooth harmonics," *Energies*, vol. 15, no. 3, p. 744, Jan. 2022.

[7] H. Yang and Y. Chen, "Influence of radial force harmonics with low mode number on electromagnetic vibration of PMSM," *IEEE Trans. Energy Convers.*, vol. 29, no. 1, pp. 38–45, Mar. 2014.

[8] R. Pile, E. Devillers, and J. Le Besnerais, "Comparison of main magnetic force computation methods for noise and vibration assessment in electrical machines," *IEEE Trans. Magn.*, vol. 54, no. 7, pp. 1–13, Jul. 2018.

[9] X. Ge, Z. Q. Zhu, G. Kemp, D. Moule, and C. Williams, "Optimal step-skew methods for cogging torque reduction accounting for three-dimensional effect of interior permanent magnet machines," *IEEE Trans. Energy Convers.*, vol. 32, no. 1, pp. 222–232, Mar. 2017.